IEEE Access
Multidisciplinary | Rapid Review | Open Access Journal

Received January 28, 2022, accepted February 28, 2022, date of publication March 8, 2022, date of current version March 17, 2022.

Digital Object Identifier 10.1109/ACCESS.2022.3157881

Wearable Multifunctional Additive Hand System for Enhancing the Workspace and Grasping Capability of the Human Hand

KANGHYEON LEE[1], PYEONG-GOOK JUNG[2], YEONSEO LEE[3], AND YOUNGSU CHA[4], (Senior Member, IEEE)

[1]Department of Mechanical and Aerospace Engineering, Seoul National University, Seoul 08826, South Korea
[2]Center for Intelligent and Interactive Robotics, Korea Institute of Science and Technology, Seoul 02792, South Korea
[3]Division of Robotics, Kwangwoon University, Seoul 01890, South Korea
[4]School of Electrical Engineering, Korea University, Seoul 02841, South Korea

Corresponding author: Youngsu Cha (ys02@korea.ac.kr)

This work was supported by the National Research Foundation of Korea (NRF) through the Ministry of Science and ICT (MSIT), Korean Government under Grant 2020R1A2C2005252 and Grant 2021M3E5D2A01023887.

ABSTRACT In this study, a wearable multifunctional additive hand (MAH) system is proposed for enhancing the workspace and grasping capability of the human hand. The MAH system consists of a main body and three fingers, and each finger has two joints. To optimize the performance, the following five parameters are considered: finger length, number of fingers, number of joints, base frame size, and joint angle range. The MAH system is designed to assist the human hand in the inward and outward modes. In the inward mode, the finger joints of the proposed system rotate in the same direction as the finger flexion of the human hand, whereas in the outward mode, the robotic fingers of the MAH system rotate in opposite directions. The proposed system provides assistive torque and expands the workspace of the human hand in the inward mode. When the additive finger joints rotate outward, they grasp an object as a third hand. The validity of the proposed system is verified analytically by changing the design parameters, considering the workspace expansion and joint torque reduction. An alpha shape is introduced to calculate the expanded workspace volume using the proposed system. The joint torque was estimated by utilizing kinematics and the force equilibrium equation, assuming that the human hand with the MAH system holds a postulated object.

INDEX TERMS Grippers and other end-effectors, human performance augmentation, multifingered hands, physically assistive devices, wearable robotics.

I. INTRODUCTION

The hand is one of the most important organs of the body throughout human history. Because human civilization has evolved with the function of the hand, modern people do most of their daily work with their hands [1]–[4]. As the society and individual roles are becoming increasingly complex, two hands with a total of ten fingers are occasionally insufficient to grasp objects of significant quantities or that are larger than the human hand [5], [6]. For instance, most mobile device users carry their devices, such as cell phones and tablet computers, continuously with their hands, which leads to a lack of empty hands.

The associate editor coordinating the review of this manuscript and approving it for publication was Pedro Neto.

Therefore, a number of research teams are interested in enhancing the capability of the human hands [7], [8]. Researchers have developed exoskeleton robots mounted on the upper body to assist the human arm and hand to produce larger forces [9]–[12]. A research team in Saga University proposed an upper limb exoskeleton robot for rehabilitation and for assisting upper body activities [9]. Noda *et al*. focused on the actuator of an upper limb robot to reduce the weight and size of the robot. They used a pneumatic electric hybrid actuator to power the robot and applied Bowden cables to the actuator. The upper limb exoskeleton robot system could assist upper body activities; however, the users may feel uncomfortable owing to the difficulty in freely moving while wearing these devices because the robots are directly mounted on the upper limbs of the human body. In addition,

they are bulky and heavy because their size is the same as the entire upper human body.

To address these problems, several studies have designed a finger exoskeleton robot that creates a torque on the finger joints or controls them to rotate in specific values of a torque, mainly for rehabilitation of the disabled [13]–[18]. For example, Lum *et al*. analyzed the application of a robotic approach to the hands of stroke patients. The finger exoskeleton robot controls finger joints and is mounted directly on top of the hand with revolute joints or elastic tendons. Therefore, the robot can damage the fingers if it malfunctions or produces excessive torque. In addition, the exoskeleton robot can only help the finger rotate its joints; thus, its application is significantly limited. Furthermore, this robot may disturb the natural movement of the finger when it is not operating because the components of these devices are made of rigid materials.

Finger-assistant exoskeletons with soft materials have also been considered [19]–[21]. However, there is a restrictive limit on the force that robotic fingers consisting of soft materials can produce. They cannot work in a multifunctional manner, such as grasping an object, and can only assist the grasping or pinching motion of the user. From another viewpoint, studies have suggested a robotic finger attached near human fingers that is referred to as the Sixth Finger [22]. Therein, the Sixth Finger consists of only one finger, located next to the pinky or on the wrist. It literally functions as the sixth finger, expanding the workspace of the hand and reducing the stress produced on a finger. However, recent studies on the design of the Sixth Finger have focused on having only one finger, thereby limiting its capability and application. It cannot grasp something by itself and can only assist the other fingers.

In this study, the MAH system is proposed to enhance the workspace as well as the grasping capability of the hand by adding three robotic fingers. The proposed system consists of a main body that plays the role of the second palm, and additive finger joints that can rotate in either the finger flexion or finger extension direction of the human hand. In other words, the fingers of the MAH system are operated in either the inward or outward directions. The main function of the MAH system is to expand the workspace of the human hand for both modes. For the inward mode, the maximum volume of objects that can be held by the hand is increased using the MAH system, and the joint torque generated by the proposed system assists in reducing the human joint torque. Furthermore, the MAH system increases the maximum weight of an object that the human finger can hold. In addition, when the finger joints of the MAH system rotate in the outward direction, the main body acts as another palm that faces the opposite direction of the human palm and can grasp an object on it with the additive fingers. To control the interaction between human body and hand robot, both sensors collecting human body signal and sensors detecting finger tip pressure are essential. A soft hand system developed by Gu *et al*. used electromyography (EMG) sensors and hydrogel-elastomer sensors [23]. They are effective in collecting electric signals from human muscle and providing feedback. The MAH system uses the piezoelectric sensor to detect signals from both human wrist skin and the target object to operate the fingers.

There are three special points of the MAH system which are distinct from other extra-digit robots: three fingers, the second palm, and the usage of the piezoelectric sensor.

- Three fingers: The current extra-digit robots are focused on assisting the performance of the human hand with only one or two robotic fingers so-called the Sixth Finger [22], [24]–[26]. They are amounted on the wrist and are operated like another thumb. Designing the MAH system, more robotic fingers are considered to have better performance to enhance the capability of the human hand. Therefore, three robotic fingers are expected to be appropriate with geometric and numerical evidences shown in Section II-B and IV-B.
- The second palm: The MAH system has the second palm and the robotic fingers which rotate in two directions. These structural features enable grasping in two spaces based on the human hand palm and the second palm. This maximizes the workspace of the human hand wearing the MAH system.
- The piezoelectric sensor: To control the additive robotic fingers, signal from the muscle represented by the EMG signal was applied [25], [26]. Therein, the devices to detect this signal were amounted on upper limbs to operate the robotic finger system. The MAH system also needs to detect the human body signal and give feedback itself to operate. Here, the piezoelectric sensors are used. The piezoelectric sensor makes electric signal as it is under strain. It controls the inward mode of the MAH system sensing the fine curve on the wrist skin when human hand grasps. In addition, the piezoelectric sensors on the tip of the robotic fingers detect whether they grasp the target object in the same way. The piezoelectric sensor is thin, light, and easy to deform so that it is considered to be proper to apply to the MAH system.

The design parameters and the overall description of the proposed system are presented in Section II. The specific values for these parameters were determined by considering the wearability while maintaining the performance of the MAH system. The hardware configuration and the mechanism of the operation modes are also indicated in Section II. The kinematic modeling and mathematical methods used for the analysis to verify the performance of the proposed system are derived in Section III. The kinematic model of the human hand and the MAH system is established geometrically using the standard Denavit-Hartenburg (DH) method [27], [28]. The force equilibrium equation is calculated to estimate the joint torque reduction, and the alpha shape is introduced to numerically measure the volume of the workspace. The results of the analysis are presented in Section IV. The performance comparison according to the variations of the parameter values is verified with the simulations, and the capability of the proposed system is also demonstrated. The workspace and reduction of torque

are achieved using MATLAB, and the delay between the detection of the grasping intention and actuator operation is obtained using a 2D tracking program. Finally, Section V concludes this study.

II. DESIGN PARAMETERS AND SYSTEM DESCRIPTION

A. FINGER LENGTH

Finger length is a main parameter and affects the workspace, system weight, and geometric constraints. Because the workspace of a system is proportional to the cube of a joint length, it is a significant parameter for determining the workspace. Although a longer joint length leads to a larger volume of the workspace, it has lower wearability. In particular, the fingers of the proposed system can interfere with human fingers or other objects. In addition, it makes it difficult to work in a narrow space, and the weight increases. For instance, if the finger length of the MAH system is too long, the entire MAH system becomes excessively heavy and inconvenient for users; there is also a possibility that the fingers of the MAH system may overlap with each other. To manage these trade-offs, the joint length was set as the maximum length that does not overlap with the other joints and human fingers. The lengths set using these criteria are $l_{M,1} = 0.045\,\text{m}$ and $l_{M,2} = 0.046\,\text{m}$, and the total length of one finger is $l_{M,T} = 0.091\,\text{m}$.

B. NUMBER OF FINGERS

The maximum number of fingers depends on the size of the actuator in each joint and the geometrical constraints. Around a human hand, there are six main extra spaces where human fingers are not located: four spaces between fingers, the space between thumb and wrist, and the space between pinky and wrist. Among these, only the space between thumb and wrist, and the space between pinky and wrist are available to locate robotic fingers because of the constraints between fingers arising in abduction/adduction movement [29]. Based on this structural characteristic of the hand, the fingers of the proposed system are considered to be placed between the thumb and wrist or between the pinky and wrist. The finger width of the system is determined by the size of the actuator; thus, there is a limit to the maximum number of fingers that can be placed on the main body.

Although more fingers provide a greater assistive torque, they increase the weight of the system and worsen wearability. The number of fingers was determined based on the fact that a minimum of three contact points would be used to hold an object in a stable manner in the outward mode. Although two fingers can hold an object, because the center of gravity is on the line between the two contact points, holding with two fingers is unstable compared to holding with three fingers.

C. NUMBER OF JOINTS

The number of joints is related to the degree of freedom (DOF). A system with a high DOF provides a greater assistive torque because more actuators are implemented and the assistive torque at the end-point is the summation of all the net torques generated by each actuator. In addition, more complex-shaped objects can be held with a high DOF system. The finger end-point of the MAH system can reach a high DOF where objects or obstacles are obstructed; thus, the workspace is also expanded. However, as the number of actuators increases, the inertia and weight of each joint also increase. Therefore, the efficiency of the assistive torque generated by each actuator decreases with a high DOF. In addition, it also limits the number of joints in which the proper length of one finger and the actuator are determined.

Considering the aforementioned, the appropriate number of joints is set to two. If a finger has two joints, the end-point is expected to cover most of the space surrounding the proposed system, while not being too heavy to use conveniently. Furthermore, several studies have reported a three-fingered hand robot design with two joints for each finger [30], [31].

D. SIZE OF BASE FRAME

The size of base frame decides the design of the other parts and is the important factor in a robotic hand system. In case of wearable devices, the size of the frame is hard to decide because it has to differ according to the body size of the wearer. If the frame size is too small, the workspace of the operating parts overlaps that of the human causing inconvenience. If the size is too big, the whole system affects the free motion of the human body and a large load is also applied to the wearer.

For this reason, the size of base frame is decided according to the size of the wearer's hand who actually operates the proposed system. The location of fingers on base frame is designed not to affect the other parts of the human hand.

E. RANGE OF JOINT ANGLE

The range of joint angle is related to the volume of the workspace. In robotic system, the types and specifications of motors as joints are really important to expect the performance because they decide the DOF and workspace of the system. Joints have to rotate in reasonable range which does not collide with the links or base frame. If joints rotate only in small range, the end point cannot reach to the target object due to the small workspace.

Six revolute joints which rotate up to 180° are considered to be suitable for configuring the fingers. This angle range is proper to make the end-points of the fingers reach both the human palm and the second palm.

F. HARDWARE DESCRIPTION

Fig. 1 presents the hardware configuration of the MAH system, which consists of the following five main parts: a main board, a second palm, switches, fingers, and a wrist sensor. All the actuators are servomotors (HS-53 Super-Economy Feather, HiTec, Inc.) and are controlled through the pulse-width modulation method by using a microprocessor unit (MCU). An Arduino Nano board with a 10-bit analog-to-digital converter is implemented in the main board as the

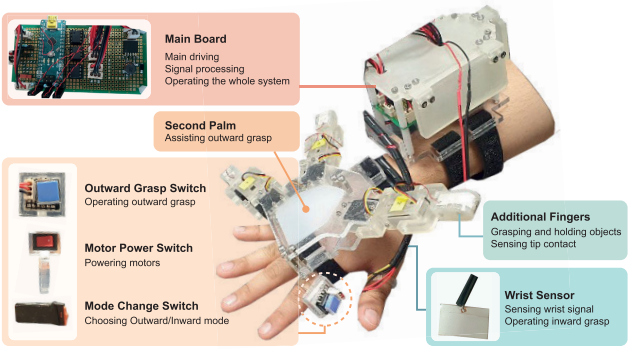

FIGURE 1. Hardware description of the MAH system.

MCU. It also receives signal outputs from the sensors on the tip of each finger and wrist.

The second palm maintains the position of the fingers. When the MAH system operates outward, the three fingers rotate outward to grasp the object on the second palm. In other words, it plays the role of an outward palm of a human. To prevent damage to an object and slippage, the tip of each finger and the second palm have surfaces made by Ecoflex (Ecoflex 00-30, Smooth-On, Inc.), which is a type of soft and flexible silicone.

The following three switches are needed to operate the MAH system: motor power, mode change, and outward grasp. The motor power switch controls the power source to supply power to the MAH system. The mode change switch determines whether the MAH system drives outward or inward. The outward grasp switch manages actuation in the outward mode.

The outward mode is controlled by an outward grasp switch. Meanwhile, the inward mode starts an operation based on the wrist sensor signal. In particular, it is operated when the output of the sensor is higher than the threshold. In inward case, the fingers of the MAH system assist the human fingers in grasping the object. In the outward mode, the MAH system grasps an object with the second palm.

There is a tip sensor on each end-point of the finger. The tip sensor detects contact with a target object through the voltage generated by the deformation of the piezoelectric sensor. The piezoelectric sensor is based on a representative piezoelectric material, polyvinylidene fluoride (PVDF) [32]–[34]. A 28 µm PVDF film was used (Measurement Specialties, Inc). The wrist sensor is also a piezoelectric sensor, which measures the curvature change of the skin on the wrist. When the human hand generates a grip, a slight curvature change occurs on the skin of the wrist [33], [35], [36]. The wrist sensor detects the change, and the main board that receives the sensor signal commands motors to rotate in the inward direction.

The hand part including fingers and the palm of the MAH system weighs 270 g. Hand exoskeleton robots were designed to have hand-mounted part which does not exceed 500 g [13], [19]–[21]. The other parts including main board, switches, and the wrist sensor weigh 310 g. Therefore, the total weight of the whole system is 580 g.

G. OPERATION MODES

The operating mechanism of the MAH system is illustrated in Fig. 2. Fig. 2(a) and 2(b) present the process in which the MAH system works in the outward and inward directions, respectively. Each mode has the five following operation steps: mode selection, object approach, object grasping, motor angle fixing, and unfolding. A detailed explanation of the outward mode process is as follows:

1) Mode selection: The outward mode is selected by the mode change switch.
2) Object approach: Target object should be placed in the workspace of the proposed system prior to the initiation of the outward grasping.
3) Object grasping: After the outward grasp switch is pushed, all six actuators rotate at a constant angular speed until the end-point is in contact with the target object.
4) Motor angle fixing: If any tip of the MAH touches the object, the piezoelectric sensor on the tip detects the contact. Then, all actuators stop rotating and fix their angle while maintaining the grasping position. The joint angle is maintained until the outward grasp switch is pressed again for release.
5) Unfolding: When the outward grasp switch is pressed, all fingers of the MAH system are unfolded and return to the initial position.

The process of the inward mode is similar to that of the outward mode; however, a few procedures are different.

1) Mode selection: The inward mode is selected with the mode change switch.
2) Object approach: The palm of the user is located on the target object.
3) Object grasping: When the user grasps the object, the wrist sensor detects the fine curvature change of the wrist skin caused by muscle contraction. When the sensor signal is higher than the threshold, all motors rotate at a constant angular speed, and the MAH system grasps the object and provides assistive torque.
4) Motor angle fixing: If any of the MAH tips touch the object, the piezoelectric sensor on the tip senses it. Then, all the actuators stop rotating and adjust their angle while maintaining the grasp posture. The joint angle is maintained until the wrist sensor detects the finger extension.
5) Unfolding: When the wrist sensor detects the finger extension, all fingers of the MAH system are unfolded and return to the initial state.

Fig. 3 presents a demonstration of the MAH system operation. The three figures in Fig. 3(a) and 3(b) present examples of the outward and inward mode operations, respectively. Fig. 3(c) shows examples for the situations in which the proposed system operating in the outward mode is necessary due to several specific constraints of the human hand. In a situation where a number of objects have to be carried at once, the MAH system can assist it by grasping rest of the objects which the human hand cannot hold more (left of

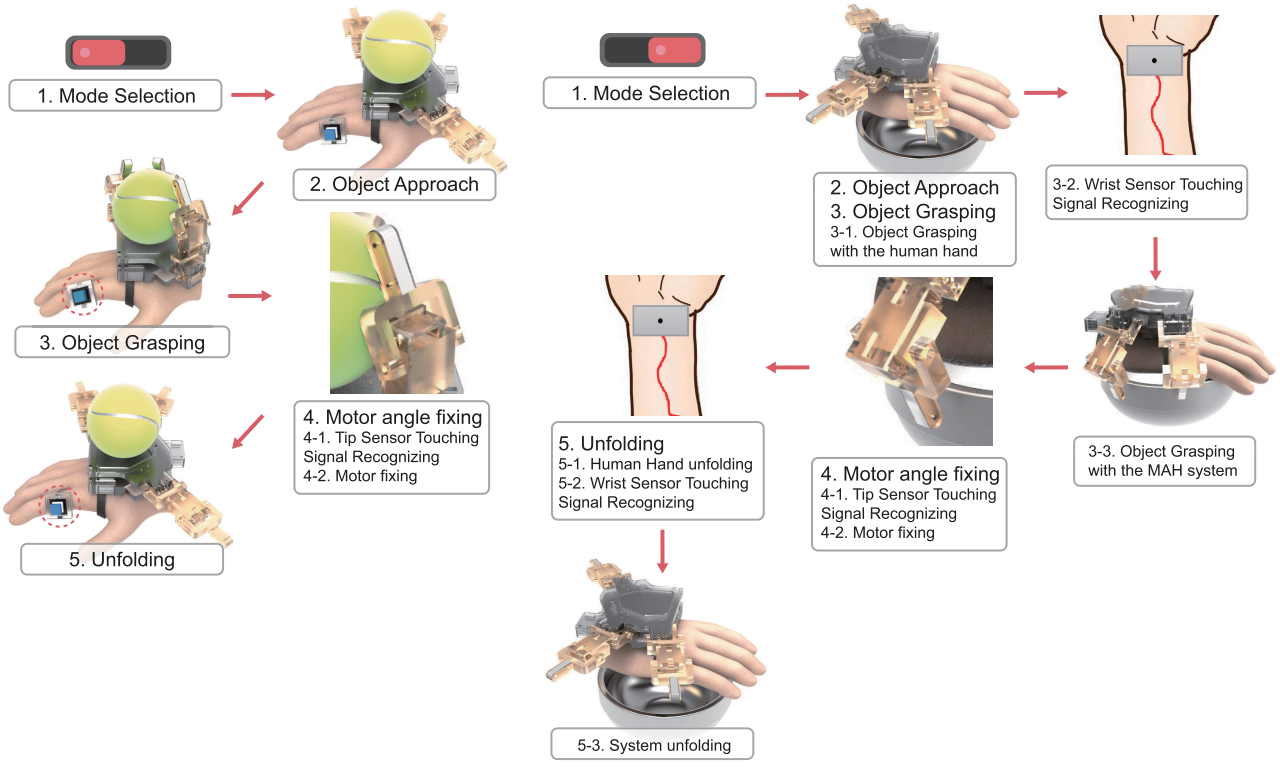

FIGURE 2. Operating mechanism when the MAH system drives (a) outward and (b) inward.

TABLE 1. Geometric values for kinematic modeling of human hand.

	Thumb	Index	Middle	Ring	Pinky
$l_{H,2}$	0.03 m	0.04 m	0.045 m	0.04 m	0.035 m
$l_{H,3}$	0.025 m	0.02 m	0.025 m	0.02 m	0.015 m
$l_{H,4}$	–	0.015 m	0.015 m	0.015 m	0.01 m
$z_{H,1}$	$-2\,^\circ \sim 10\,^\circ$	$-10\,^\circ \sim 20\,^\circ$	$-10\,^\circ \sim 20\,^\circ$	$-10\,^\circ \sim 20\,^\circ$	$-10\,^\circ \sim 20\,^\circ$
$z_{H,2}$	$-80\,^\circ \sim -30\,^\circ$	$-15\,^\circ \sim 85\,^\circ$	$-15\,^\circ \sim 85\,^\circ$	$-15\,^\circ \sim 85\,^\circ$	$-15\,^\circ \sim 85\,^\circ$
$z_{H,3}$	$-90\,^\circ \sim -10\,^\circ$	$0\,^\circ \sim 90\,^\circ$	$0\,^\circ \sim 90\,^\circ$	$0\,^\circ \sim 90\,^\circ$	$0\,^\circ \sim 90\,^\circ$
$z_{H,4}$	–	$0\,^\circ \sim 70\,^\circ$	$0\,^\circ \sim 70\,^\circ$	$0\,^\circ \sim 70\,^\circ$	$0\,^\circ \sim 70\,^\circ$

TABLE 2. Geometric values for kinematic modeling of MAH system.

$l_{M,1}$	0.045 m
$l_{M,2}$	0.046 m
$z_{M,1}$	$-90\,^\circ \sim 90\,^\circ$
$z_{M,2}$	$-90\,^\circ \sim 90\,^\circ$

Fig. 3(c)). The proposed system can also be helpful when the human hand has restrictions. For instance, human fingers are fixed to the bandage when they are injured (middle of Fig. 3(c)). In another case, human hands have to be protected when hygiene is important such as in laboratory or infectious diseases situation (right of Fig. 3(c)). In these situations, the MAH system can perform tasks which the human hand does instead of it operating in the outward mode.

III. KINEMATICS AND JOINT TORQUE ESTIMATION FOR ANALYSIS

A. GEOMETRY AND COORDINATE SYSTEM

To verify the performance of the proposed system analytically, kinematic modeling of the human hand and the MAH system was performed. The origin and coordinates are shown in Fig. 4. Fig. 4(a) presents the coordinates and kinematic scheme of the right human hand. The index, middle, ring, and pinky fingers consist of spherical joints, two revolute joints, an end-point, and three links, respectively. The thumb consists of a spherical joint, a revolute joint, an end-point, and two links. The origin of the coordinate is on the first joint of the middle finger (see blue axes in Fig. 4(a)), and the positions of the first joints of the other fingers were predefined by the size of the subject's hand.

Fig. 4(b) presents the coordinates and kinematic scheme of the MAH system. The prototype has three identical fingers, and each finger has two links and two revolute joints. As indicated in Section II, a possible position for the additive fingers is between the thumb and wrist, or pinky and wrist. The locations of the first joints are determined according to the possible positions considering the size of the actuators. The origin of the MAH system coordinates are the same as

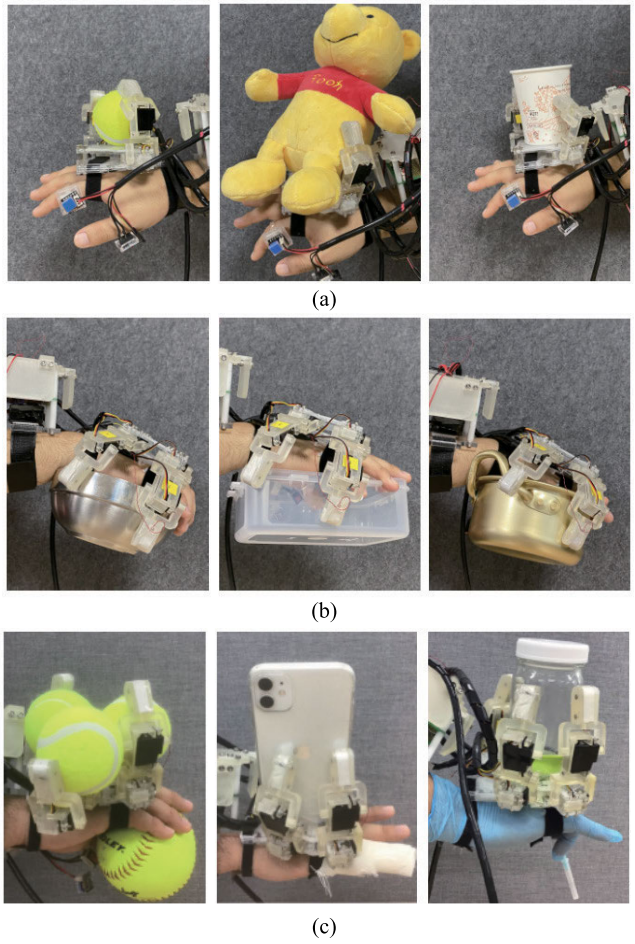

FIGURE 3. Examples of the MAH system operation; (a) outward mode, (b) inward mode, and (c) cooperation between the human hand and the MAH system in outward mode.

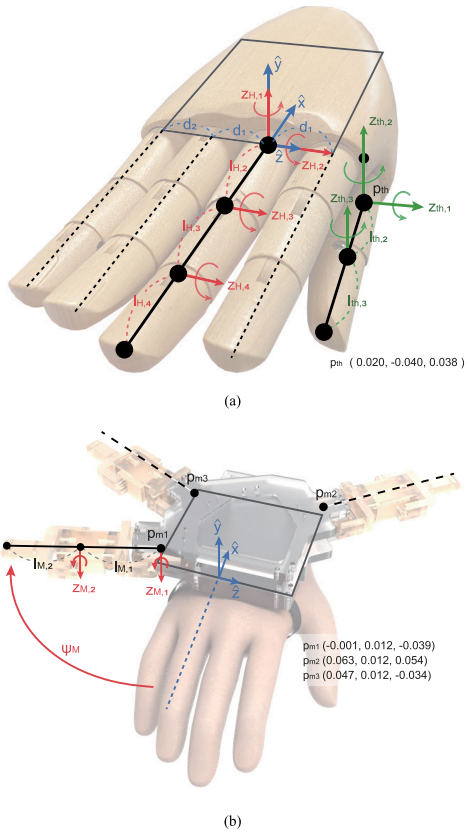

FIGURE 4. (a) Kinematic modeling of the human hand and (b) the MAH system. The origin and coordinates of these two are the same. The origin is on the first joint of the middle finger.

that of the human hand. Specific values of each length and the range of joint angles for the human hand and the MAH system are shown in Tables 1 and 2, respectively. In Table 1, index H consists of *th*, *in*, *mi*, *ri*, and *pi*, which indicate the thumb, index, middle, ring, and pinky fingers, respectively ($H = \{th, in, mi, ri, pi\}$). In Table 2, index M consists of $m1$, $m2$, and $m3$, which refer to fingers 1, 2, and 3 of the MAH system, respectively ($M = \{m1, m2, m3\}$). The geometric values of the human hand are modeled based on a previous study [37].

The size and shape of the palm of the MAH system are determined by referring to the subject's hand and the considered parameters. The geometric values not shown in the tables and figures are as follows: $d_1 = 0.018$ m, $d_2 = 0.016$ m, $\psi_{m1} = -76.19°$, $\psi_{m2} = -127.47°$, and $\psi_{m3} = -116.00°$. ψ_M is the angle between the direction of finger M and the x-axis of the origin.

B. DENAVIT-HARTENBURG PARAMETERS

The strategy to find the end point trajectories of all fingers consists of two steps as follows:

TABLE 3. DH parameters of human hand thumb.

i	θ_i	d_i	a_i	α_i
1	$180° + z_{th,1}$	0	0	0
2	0	0	0	90 °
3	$z_{th,2}$	0	$l_{th,2}$	0
4	$z_{th,3}$	0	$l_{th,3}$	0

1) Find the trajectory of the end point with the first joint positioned at the origin.
2) Translate the trajectory by the displacement between the first joint and the origin.

The standard DH method was introduced to derive the kinematics for each finger of both the human hand and the MAH system. Standard DH convention assumes that the i^{th} coordinate frame is at the $(i+1)^{th}$ joint. The coordinate transformation is represented by four DH parameters, and the transformation matrix is as follows:

$$T_{i-1}^{i} = \begin{bmatrix} cos(\theta_i) & -sin(\theta_i)cos(\alpha_i) & sin(\theta_i)sin(\alpha_i) & a_i cos(\theta_i) \\ sin(\theta_i) & cos(\theta_i)cos(\alpha_i) & -cos(\theta_i)sin(\alpha_i) & a_i sin(\theta_i) \\ 0 & sin(\alpha_i) & cos(\alpha_i) & d_i \\ 0 & 0 & 0 & 1 \end{bmatrix} \quad (1)$$

where θ_i is the joint angle between the x_{i-1} and x_i axis about the z_{i-1} axis, and d_i is the distance from the origin of the $(i-1)^{th}$ frame to the x_i axis along the z_{i-1} axis. Moreover, a_i is the offset distance between the z_{i-1} and z_i axis along the x_i axis, and α_i is the angle from the z_{i-1} axis to the z_i axis about the x_i axis.

The vector of the end-point, $\mathbb{P}$, is obtained using the following equations, which are a series of transformation matrices:

$$T_0^n = T_0^1 T_1^2 T_2^3 \cdots T_{n-1}^n \tag{2}$$

$$P' = T_0^n \begin{bmatrix} 0 \\ 0 \\ 0 \\ 1 \end{bmatrix} + Q \in \mathbf{R}^4 \tag{3}$$

where n is 4 for the human thumb and 5 for the other human fingers, as well as for the fingers of the MAH system. The DH parameters of the human hand and MAH system are shown in Table 3, 4, and 5. The last component of P' is always 1 because it is added to match the dimension of the equation. Therefore, $\mathbb{P}$ consists of the first three components of P'.

Q is the parallel translation matrix, and its value is $[0.02\ -0.04\ 0.038\ 0]^T$, $[0\ 0\ d_1\ 0]^T$, $[0\ 0\ 0\ 0]^T$, $[0\ 0\ -d_1\ 0]^T$, and $[0\ 0\ -d_1\text{-}d_2\ 0]^T$ for the thumb, index, middle, ring, and pinky fingers, respectively. For the MAH system, Q is $[-0.001\ 0.012\ -0.039\ 0]^T$, $[0.063\ 0.012\ 0.054\ 0]^T$, and $[0.047\ 0.012\ -0.034\ 0]^T$ for fingers 1, 2, and 3, respectively. The (4,1) component of matrix Q, 0, is a meaningless number. The first joints of all human fingers are spherical joints that consist of two revolute joints each; thus, they were considered to have two DH parameters set, and $l_{H,1}$ was zero.

TABLE 4. DH parameters of human hand index, middle, ring, and pinky finger.

i	θ_i	d_i	a_i	α_i
1	180 °	0	0	90 °
2	$z_{H,1}$	0	0	−90 °
3	$z_{H,2}$	0	$l_{H,2}$	0
4	$z_{H,3}$	0	$l_{H,3}$	0
5	$z_{H,4}$	0	$l_{H,4}$	0

TABLE 5. DH parameters of MAH system finger.

i	θ_i	d_i	a_i	α_i
1	180 °	0	0	90 °
2	ψ_M	0	0	0
3	0	0	0	−90 °
4	$z_{M,1}$	0	$l_{M,1}$	0
5	$z_{M,2}$	0	$l_{M,2}$	0

C. CONTACT POINT DETECTION

Contact points are detected prior to torque estimation because the required torque varies depending on the position of the contact point. To estimate the joint torque under the same condition, a spherical object is postulated, which has the following properties:

- Shape: Sphere
- Radius: 0.04 m
- Material: ABS Alloy
- Density: 982.91 kg/m^3

The equations obtained from the inverse kinematics based on the aforementioned kinematic modeling are inconsistent, except for the thumb, owing to the difference between the number of unknowns, which are the components of the position vector, as well as the equations, which indicate the number of unknown DH parameters. Therefore, the contact point was calculated kinematically using the following assumptions and criteria.

1) All fingers can approach any point on the sphere without obstruction by the object.
2) Points are calculated kinematically with a distance of 3×10^{-5} m, i.e. 0.03 mm, or less between the points and the surface of the postulated object.
3) As the direction of the force vector moves closer to the opposite direction of gravity, the required joint torque decreases because only the gravity of the object needs to be compensated to make the resultant force zero. Therefore, the point with the lowest y-axis coordinate value among the points that satisfy the previous criteria is selected as the contact point.

D. JOINT TORQUE ESTIMATION

One of the main contributions of the proposed system is joint torque assistance. To estimate the generated joint torque by simulation, the joint torque was analyzed based on the following assumptions.

1) There is no friction on the surface of the target sphere object.
2) The torque generated by each actuator has the same magnitude, 0.187×10^{-3} N·m, which is 1/1000 of the stall torque. In other words, the actuator operates with a constant input without a controller and feedback.
3) All contact forces are directed to the center of the target object. Therefore, the unit force vector, $\mathbb{U}_X$, is $(O - C_X)/\|O - C_X\| \in \mathbf{R}^{3\times 8}$, where O is the position of the target object's center, and C is the position of the detected contact point. Index X is the set of the human fingers and the fingers of the MAH system, and $X = \{H, M\}$.
4) The percentage contribution of the four fingers, excluding the thumb, while grasping an object is constant; the values are derived from a previous study [38].

The Jacobian matrix of each finger in the MAH system is obtained from the transformation matrix and the joint angles of the contacting situation. For the convenience of calculation, ψ_M is set to zero, and there is no z-axis force component.

Thus, the relationship between the contact force vector and joint torque is as follows:

$$\begin{bmatrix} \tau_{M,1} \\ \tau_{M,2} \end{bmatrix} = J_M^T \mathbb{F}_M \tag{4}$$

where $\tau_{M,1}$ and $\tau_{M,2}$ are the torque produced by the first joint of the finger in the MAH system and that produced by the second joint of the finger in the MAH system, respectively. Moreover, J_M is the Jacobian matrix of the MAH system ($J_M \in \mathbf{R}^{2\times 2}$), and $\mathbb{F}_M$ is the end-point force of the finger in the MAH system ($\mathbb{F}_M \in \mathbf{R}^2$). The torque produced by an actuator of the MAH system is fixed at 0.187×10^{-3} N·m based on an assumption. Therefore, this matrix equation becomes two equations that have two unknowns and can be solved. The magnitude of force produced by the end-point of each finger, $\|\mathbb{F}_M\|$, was also obtained. Because the force generated by the MAH system is calculated and the percentage contribution of the four fingers is constant, the force equilibrium equation can be expressed as follows:

$$\begin{bmatrix} 0 \\ 0 \\ 0 \end{bmatrix} = [\mathbb{U}_X] \begin{bmatrix} \|\mathbb{F}_{th}\| \\ r \cdot f_{in} \\ r \cdot f_{mi} \\ r \cdot f_{ri} \\ r \cdot f_{pi} \\ \|\mathbb{F}_{m1}\| \\ \|\mathbb{F}_{m2}\| \\ \|\mathbb{F}_{m3}\| \end{bmatrix} \tag{5}$$

where f_{in}, f_{mi}, f_{ri}, and f_{pi} are the percentage contribution and constant. In Equation (5), there are three linear equations and two unknown variables, $\|\mathbb{F}_{th}\|$ and r. Therefore, instead of r, two variables, k and p, were introduced, which were observed not to have distinctly different values during all the calculations. The force equilibrium equation with variables is

$$\begin{bmatrix} 0 \\ 0 \\ 0 \end{bmatrix} = [\mathbb{U}_X] \begin{bmatrix} \|\mathbb{F}_{th}\| \\ k \cdot f_{in} \\ k \cdot f_{mi} \\ p \cdot f_{ri} \\ p \cdot f_{pi} \\ \|\mathbb{F}_{m1}\| \\ \|\mathbb{F}_{m2}\| \\ \|\mathbb{F}_{m3}\| \end{bmatrix} \tag{6}$$

The transformation matrix and Jacobian for the human fingers are also found. Therefore, there is a relationship between the torques produced by the human fingers and their contact forces as shown in Equation (7):

$$\begin{bmatrix} \tau_{H,1} \\ \tau_{H,2} \\ \tau_{H,3} \\ \tau_{H,4} \end{bmatrix} = J_H^T \mathbb{F}_H \tag{7}$$

where $\tau_{H,1}$, $\tau_{H,2}$, $\tau_{H,3}$, $\tau_{H,4}$, J_H, and $\mathbb{F}_H$ are the torque produced by the first, second, third, and fourth joints of the human finger, the Jacobian matrix of the human finger ($J_H \in \mathbf{R}^{3\times 4}$), and the end-point force of the human finger ($\mathbb{F}_H \in \mathbf{R}^3$), respectively ($\tau_{H,4}$ does not exist for the thumb owing to the kinematic model. Thus, J_H, is a 3×3 matrix). The torque that each human finger must produce to hold the target sphere is estimated with this equation.

TABLE 6. Volume of the workspace by the number of joints.

The number of joints	Volume of the workspace
2	42.5×10^{-4} m^3
2′	54.0×10^{-4} m^3
3	72.1×10^{-4} m^3

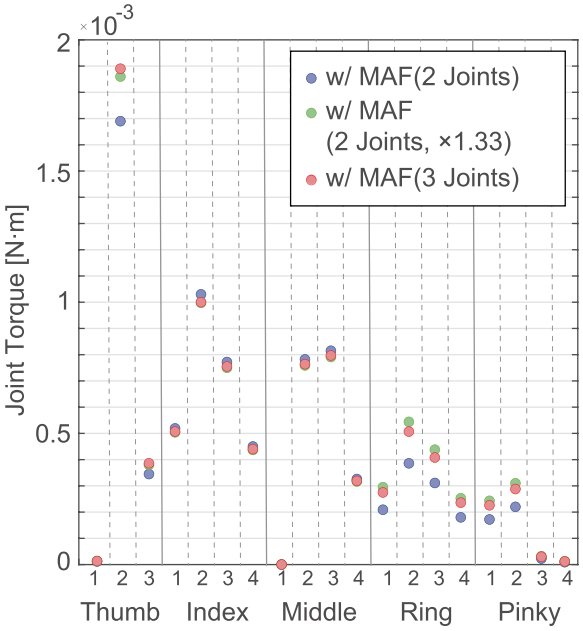

FIGURE 5. Human finger joint torque reduction by the number of finger joints in the MAH system. Blue, green, and red points are estimated joint torque for the case of two joints, 2′ joints (two joints with 1.33 times long links), and three joints, respectively. Left to right of each area separated by vertical line is the first, second, third, and fourth (the thumb has no fourth joint) joints.

IV. ANALYSIS OF SIMULATION AND EXPERIMENTAL RESULTS

The performance of the proposed system was verified by comparing the expanded workspace and reduction of the human finger joint torque based on the kinematic modeling in Section III. The performance of the MAH system according to five parameters was also analyzed considering the volume of the workspace and reduction of the torque on the human finger by the MAH system. To numerically analyze the volume of the workspace, an alpha shape is introduced [39]–[42], which is a family of the linear simple curves that contains a finite number of points in the Euclidean plane. The alpha shape is useful in calculating the area or volume of an irregular shape, which consists of a finite number of points. Because the kinematic modeling of the human hand has 19-DOF and

that of the human hand with the MAH system has 25-DOF, the workspace has an irregular shape. Therefore, the volume of the workspace was achieved by the `alphaShape.m` function of MATLAB (Matlab2019b, MathWorks, Inc.).

To operate the MAH system in the inward mode, the grasp motion is detected by the piezoelectric sensor on the wrist. The piezoelectric sensor signal that occurs on the wrist is measured by the MCU on the main board, followed by the actuators being operated by the process in the MCU with the sensor output. Therefore, there is an inevitable delay between the occurrence of the sensor signal and motor rotation. In other words, the delay between the grasping intention detection and actuator operation occurs. This delay is determined because synchronization affects the effectiveness of the assistive torque generated by the MAH system. To measure the delay, a vision camera (DSC-RX10M3, Sony Corp.) was utilized as an observer of the MAH system operation to detect the actuator operation by using a 2D tracking program (ProAnalyst Motion Analysis Software, Xcitex, Inc.). The operation was recorded using a camera with a rate of 240 fps. Three points were marked on two joints and the end-point to be detected by the tracking program. To synchronize the measurements from the piezoelectric sensor and vision camera, an LED lights up using an MCU on the MAH system.

A. ANALYSIS IN TERMS OF THE NUMBER OF JOINTS

The MAH system has two links with lengths of 0.045 m and 0.046 m each, and the proposed system was compared with a system that was assumed to have three joints for each finger with a length of 0.030 m. The length of the additional link does not contact the MAH palm when all the joints rotate as the maximum angle. To have the same conditions as the three-joint case, excluding the number of joints, two joints with the total length of each finger being the same as the total length of the three joints were also considered. Thus, the lengths of the two links in case $2'$ are 0.121 m and 1.33 times with respect to the length of the two links in case 2.

An analysis of the assistive torque is shown in Fig. 5. The y-axis is the joint torque generated by the human hand. Therefore, the lower joint torque indicates that the proposed system better assists the wearer. For the index, ring, and pinky finger, the second joint, $z_{H,2}$ has the highest value of joint torque. This tendency is also appeared in other researches studying human finger joint torque. The index and middle finger joint torque generated by the human hand for the case with three joints is 0.6 % larger than that for the case with $2'$ joints on average. In addition, the ring finger and pinky joint torque generated by the human hand in the case of three joints is 31.3 % larger than that in the case of two joints on average. In other words, the torque assisted by the case of three joints on the index finger and middle finger is less than that of the $2'$ joints, and that on the ring finger and pinky is less than that of the two joints. The smallest reduction of torque on the thumb among the three cases is also shown. The thumb joint torque in the case of three joints is 11.8 % larger than that of the case with two joints, and 1.6 % larger than that of the case with $2'$ joints.

The volume of the workspace for each case is shown in Table 6, which presents that the case with three joints has a workspace volume 1.696 times larger than that of the case with 2, and 1.34 times larger than that of the case with $2'$. The case with three joints is apparently more efficient in terms of workspace; however, there is no significant increase in terms of assistive torque, while it consists of approximately 50 % more weight than that of the case with two joints.

TABLE 7. Volume of the workspace by the number of fingers.

The number of fingers	Volume of the workspace
2	$34.0 \times 10^{-4}\,\mathrm{m}^3$
3	$42.5 \times 10^{-4}\,\mathrm{m}^3$
4	$47.0 \times 10^{-4}\,\mathrm{m}^3$

B. PERFORMANCE FOR VARIOUS NUMBERS OF FINGERS

The proposed system has three fingers, one between the thumb and wrist and two between the pinky and wrist. Additionally, a simulation system with two and four fingers is compared with the proposed system. For the two-finger system, the addition of the finger between the thumb and wrist is removed from the proposed system. For the four-finger system, one finger is added between the thumb and index finger to the proposed system. The three systems, including the proposed system, are also analyzed considering the workspace and torque reduction.

Table 7 presents the volume of the workspace for the three cases. For the two-finger system, the volume of the workspace is approximately 0.80 times that of the proposed system, which has three fingers. For the four-finger system, the volume of the workspace is approximately 1.11 times that of the proposed system. In other words, the increase rate of the workspace volume from the two-finger system to the three-finger system, which is 25.0 %, is more efficient than when adding one finger from three fingers, which is 10.6 %.

The results of the joint torque analysis are shown in Fig. 6, which indicate that the case of the three fingers reduces the largest torque. The two-finger MAH system presents the smallest torque reduction as expected, and the four-finger MAH system follows. The three-finger MAH system presents a remarkable ability to assist in grasping a target object among the three cases. The main reason the joint torque with the three-finger system is more reduced than the joint torque with the four-finger system is because the magnitude of the force independent of the direction of gravity is increased. In other words, the magnitude of the x-direction and z-direction forces with the three-finger system is the smallest among the three systems, and reduces the joint torque on the human finger in the holding situation.

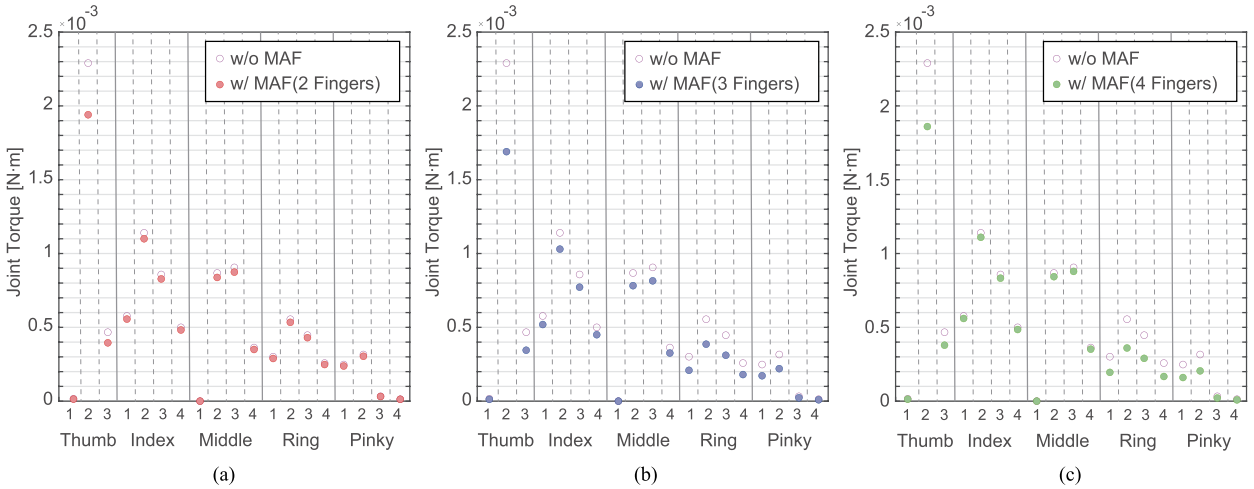

FIGURE 6. Torque of the human fingers by simulation to hold the target sphere with and without the MAH system in three cases. The hollow circles on the graphs are estimated joint torque without the MAH system. The red, blue, and green points are estimated joint torque with two, three, and four-finger system, respectively. Left to right of each area separated by vertical line is the first, second, third, and fourth (thumb has no fourth joint) joints.

In summary, compared to the weight of a system increase due to the addition of fingers, the three-finger system, which is the proposed system, effectively increases the volume of the workspace while reducing the human finger joint torque the most.

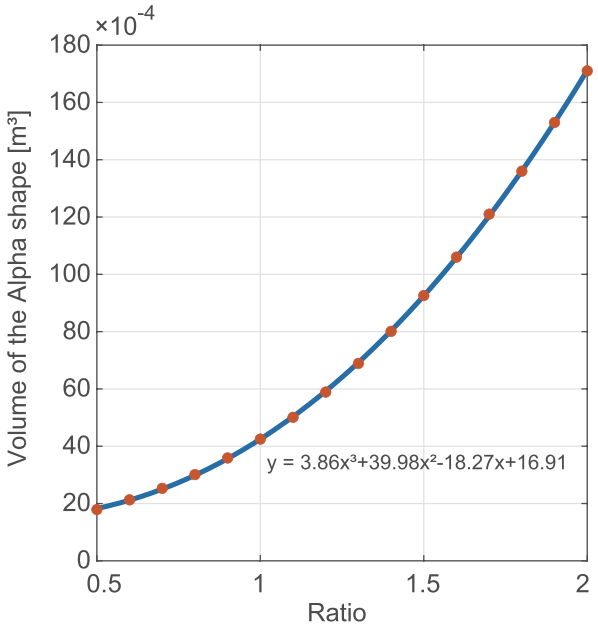

FIGURE 7. The volume of the workspace of the human hand with the MAH system along with the finger length of the MAH system. The red points are the volume of the workspace data according to change of the finger length of the MAH system. The blue line represents poly-fitted results by 3rd-order polynomial.

C. WORKSPACE ANALYSIS ACCORDING TO THE FINGER LENGTH

The lengths of the two links in the prototype are 0.045 m and 0.046 m. The ratios of the link lengths of the additional cases to the original lengths were considered from 0.5 to 2.0 with 0.1 intervals. Because volume is proportional to the cube of the length, the result was fitted to third polynomials.

The analysis results are shown in Fig. 7. Note, the finger length of the MAH system was determined as the maximum length that does not interfere with the other fingers for wearability, despite the workspace increasing in proportion to the cube of the length, as shown in the figure.

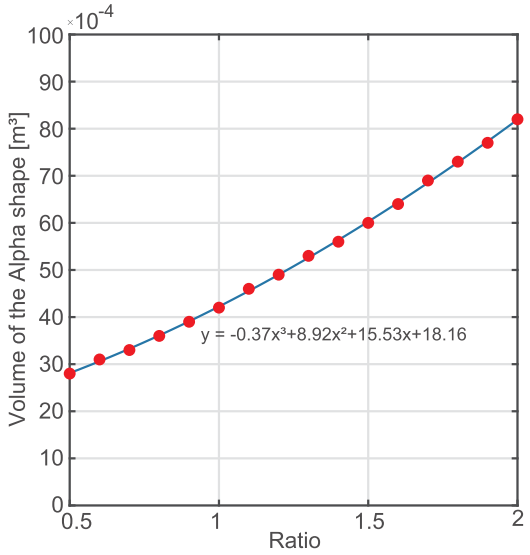

FIGURE 8. The volume of the workspace of the human hand with the MAH system along with the distance between the origin of the MAH system and the fingers. The red points are the volume of the workspace data. The blue line represents poly-fitted results by 3rd-order polynomial.

D. WORKSPACE ANALYSIS ACCORDING TO THE BASE FRAME SIZE

For the prototype of the MAH system, the three fingers are located by coordinates, Q, which is proposed in Equation (3). The ratios of the changed distances between the origin of

the kinematic modeling of the MAH system and its fingers to the original ones were considered from 0.5 to 2.0 with 0.1 intervals. Because volume is proportional to the cube of the length, the result was fitted to third polynomials as shown in Fig. 8.

Fig. 8 shows the analysis results of the workspace. As the fingers of the MAH system are located further from the origin, the workspace of the system becomes larger in proportion to the cube of the distance. However, as the base frame becomes larger, the whole system becomes bulkier and more load applies to the human hand. In addition, if base frame is designed to be larger than the hand of the wearer, it affects the space around the human hand where the hand can reach. For this reason, the size of base frame is determined as the size of the wearer's hand.

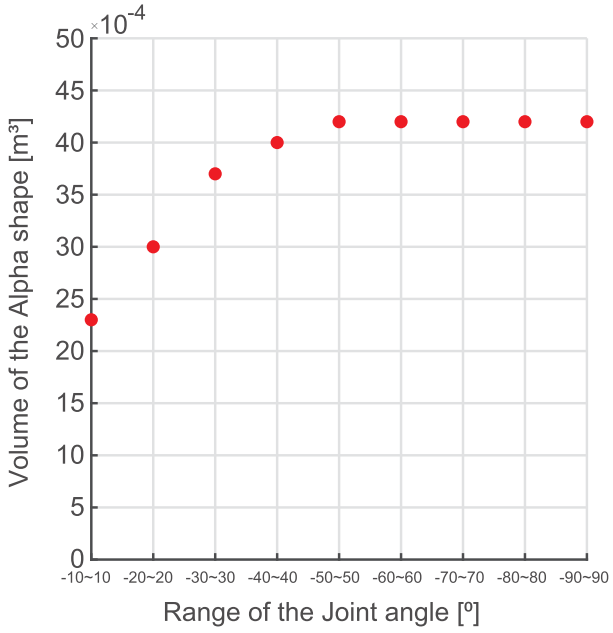

FIGURE 9. The volume of the workspace of the human hand with the MAH system along with the range of the joint angle. The red points are the volume of the workspace data according to the change of the joint angle of the motors used in the MAH system.

E. WORKSPACE ANALYSIS ACCORDING TO THE JOINT ANGLE RANGE

Fig. 9 shows the change of the workspace according to the change of the joint angle range. The prototype of the MAH system has joints whose angle range is $-90°$ to $90°$. The limits to the maximum/minimum value of the joint angle is considered from $-10°/10°$ to the $-90°/90°$ with $-10°/10°$ intervals. The workspace increases as the joint angle range increases until the range reaches to $-50°$ to $50°$. The graph shows that it has maximum values, 42.5×10^{-4} m^3, which is the volume of the workspace of the prototype. Though, less than $-90°/90°$ of rotation restricts the end-point of the fingers so that they cannot grasp things whose height is smaller than a link of the fingers. Thus, joint rotating $-90°/90°$ is proper to grasp things of various shape and size.

F. PERFORMANCE OF THE PROPOSED SYSTEM

Based on the modeling of the human hand and the MAH system in Section III, the workspace of the human hand with and without the MAH system are presented in Fig. 10. The upper row of Fig. 10 presents the workspace of the human hand, while the lower row of Fig. 10 presents the workspace of the human hand and the MAH system. The overall workspace with and without the MAH system is expressed in the first column of Fig. 10. The second, third, and last columns of Fig. 10 are the projections on the xy, yz, and xz planes, respectively. The indigo, green, magenta, light blue, and yellow colored areas indicate the workspace of the thumb, index, middle, ring, and pinky fingers, respectively. The blue, brown, and dark blue colored areas display the workspace of fingers 1, 2, and 3 in the MAH system.

To quantify the volume of the workspace, the volume of the workspace with and without the MAH system was calculated using the alpha shape, which was plotted using MATLAB and is presented in Fig. 11. The volume of the workspace of the human hand was 2.38×10^{-4} m^3, and that of a human hand wearing the MAH system in the inward mode is 20.00×10^{-4} m^3. In other words, the workspace is expanded by approximately 8.40 times. In the outward mode, the workspace of the MAH system was 9.63×10^{-4} m^3.

Fig. 12 presents the estimated joint torque of the human fingers required to hold the target sphere object with and without the MAH system. The MAH system distinctly reduces the joint torque on all five fingers. The degree of reduction for the fingers is 26.21 %, 9.93 %, 10.08 %, 30.42 %, and 30.44 % for the thumb, index, middle, ring, and pinky fingers, respectively. In other words, the reduction efficiency of the MAH system is in the order of pinky finger, ring finger, thumb, middle finger, and index finger. The average reduction rate is approximately 21.14 %. The total amount of torque reduced by the MAH system is approximately 1.91×10^{-3} N·m.

G. DELAY MEASUREMENT THROUGH GRASPING INTENTION DETECTION

Fig. 13 presents the results of the delay experiment. The delay is the difference between the time when the sensor signal reaches the threshold value and when the node starts to move. Four delays, which are the delays of the two actuators on one finger of the MAH system while grasping and unfolding, were measured. The results of ten experiments are presented in Table 8. The average delay time is approximately 0.048 s.

H. DESIGN OPTIMIZATION

In Section II, the prototype design and the five parameters (finger length, number of fingers, number of joints, base frame size, and joint angle range) for the MAH system are decided based on valid grounds. Finger length and base frame size are set so that there is no collision between fingers. The number of fingers is chosen to be three considering the minimum contact points with the target object. The number

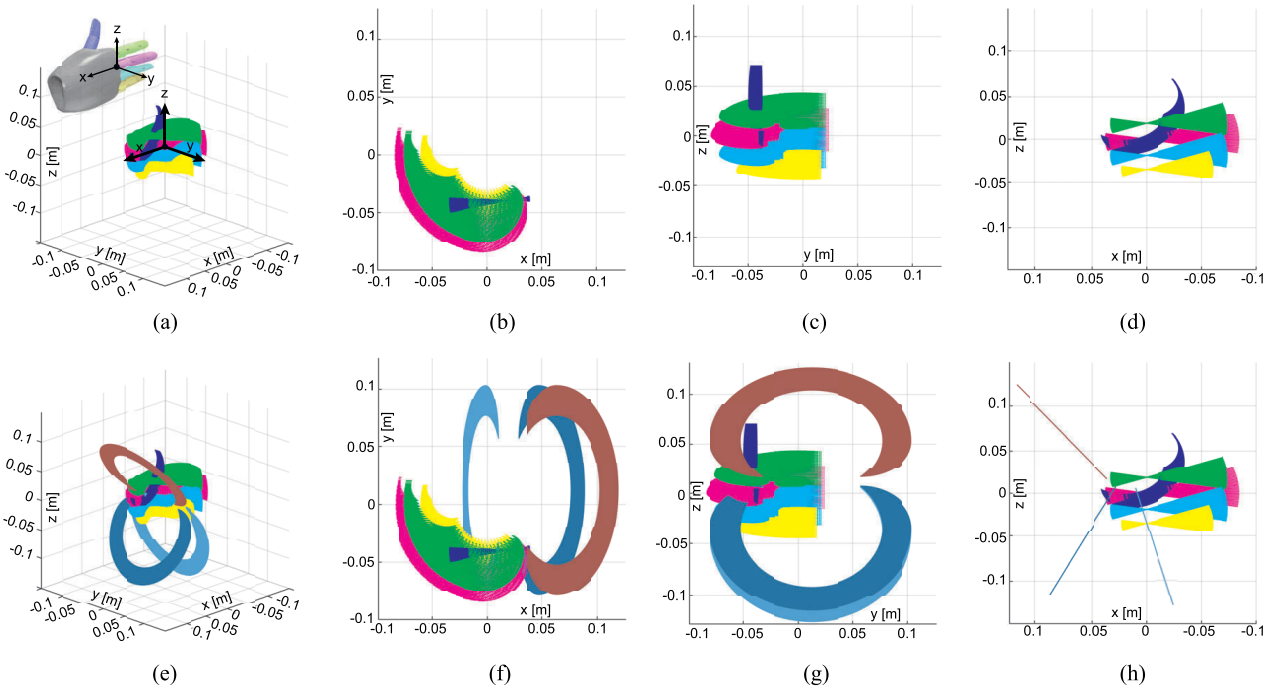

FIGURE 10. Workspace trajectory of a human hand without the MAH system ((a), (b), (c), (d)), and a human hand with MAH ((e), (f), (g), (h)). (a) and (e) are workspace in a 3D dimensional space, (b) and (f) are projection in xy plane, (c) and (g) are in yz plane, and (d) and (h) are in xz plane. In the graphs showing the workspace of human hand, indigo, green, magenta, light blue, and yellow area are the workspace of the thumb, index, middle, ring, and pinky fingers, respectively. The blue, brown, and dark blue areas shown in the graphs are the workspace of fingers 1, 2, and 3 in the MAH system, respectively.

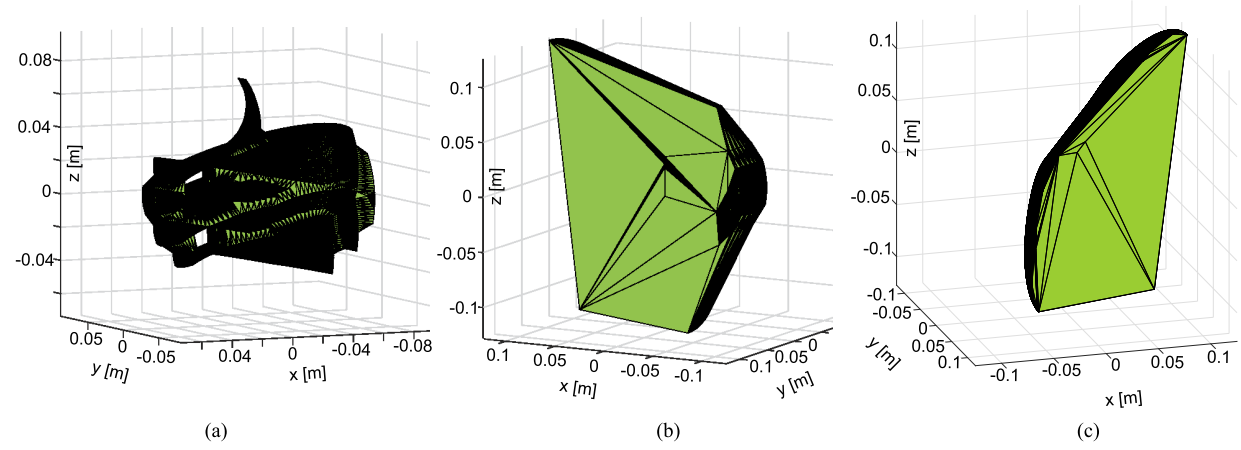

FIGURE 11. (a) Alpha shape of the human hand without the MAH system, (b) the human hand with the MAH system in the inward mode, and (c) the MAH system in the outward mode.

of joints and joint angle range are set not to collide each other but to make maximum volume of workspace.

In Section IV, the validity of the prototype is confirmed by conducting parameter study. The results of the analysis for number of joints, number of fingers, and joint angle range demonstrate that the design of the prototype which has three fingers with two joints rotating from $-90°$ to $90°$ presents the better performance than the any other additional case. In case of finger length and base frame size, the workspace volume of the MAH system increases as those two parameters increase. However, structural and weight problems arise if the parameters become too big. Therefore, the upper limits are necessary. Two links that are 0.045 m and 0.046 m long, and base frame that is 5.859×10^{-3} m^2 wide, as same as those of the prototype, are verified to be appropriate for the limit.

Briefly, the optimized design parameters are as follows:

- Finger length: 0.091 m (0.045 m and 0.046 m for each link)

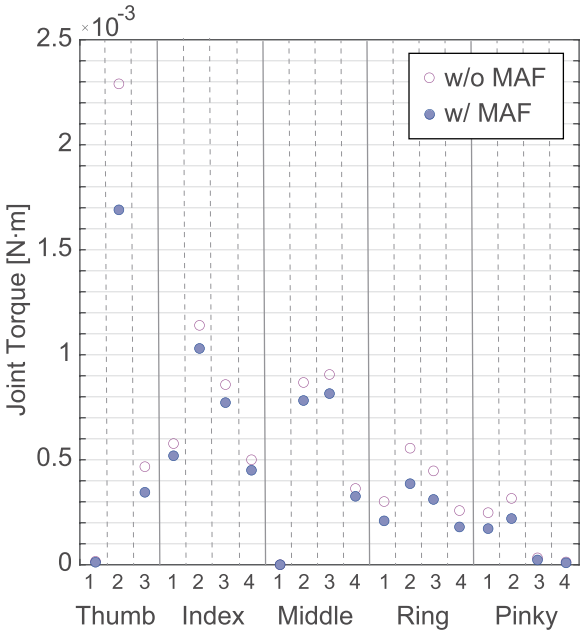

FIGURE 12. Estimated human hand joint torque to hold the target sphere with and without the MAH system. The hollow circles represent the estimated joint torque when the human hand holds the sphere, and the blue circles represent the data of torque when the human hand holds the sphere with assistance of the MAH system. Left to right of each area separated by vertical line is the first, second, third, and fourth (thumb has no fourth joint) joints.

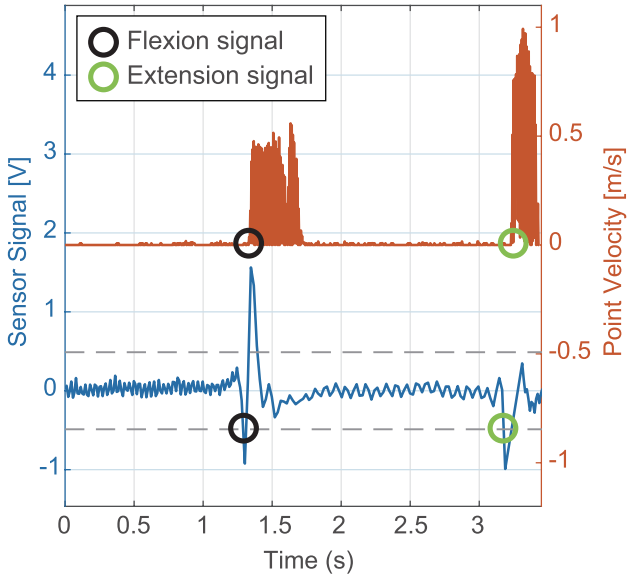

FIGURE 13. Piezoelectric sensor signal on the wrist and the velocity of a node on the finger of the MAH system when the MAH system is in the inward mode. Red line represents the velocity of a node on the joint of the MAH system, and the blue line represents the piezoelectric sensor signal on the wrist, respectively. The first delay time occurs when the MAH system grasps, and the second delay time occurs when the fingers of the MAH system are unfolded.

- Number of fingers: Three
- Number of joints: Two
- Base frame size: 5.859×10^{-3} m^2
- Joint angle range: $-90°$ to $90°$

TABLE 8. Wrist sensor signal delay.

	Grasping		Unfolding	
	1st joint	2nd joint	1st joint	2nd joint
1	0.043 s	0.043 s	0.056 s	0.048 s
2	0.033 s	0.033 s	0.041 s	0.032 s
3	0.057 s	0.057 s	0.062 s	0.045 s
4	0.037 s	0.045 s	0.048 s	0.048 s
5	0.068 s	0.068 s	0.08 s	0.071 s
6	0.03 s	0.03 s	0.042 s	0.026 s
7	0.021 s	0.021 s	0.068 s	0.06 s
8	0.039 s	0.039 s	0.069 s	0.052 s
9	0.048 s	0.057 s	0.07 s	0.062 s
10	0.048 s	0.048 s	0.045 s	0.045 s
Average	0.0424 s	0.0441 s	0.0581 s	0.0489 s

V. CONCLUSION

In this study, the MAH system was proposed as a method to enhance the capability of the human hand. The two main functions of the MAH system are to expand the workspace of the human hand and to reduce the generated joint torque of the human fingers when the fingers grasp an object.

The finger length, number of fingers, number of joints, the base frame size, and the range of the joint angle were considered as the design parameters. To verify the validity of the design of the MAH system, a simulation using a kinematic model was conducted. Based on the two main effects expected, the optimal volume of the workspace and the joint torque of the human hand with the MAH system according to the changes in the five parameters were determined analytically with MATLAB. The DH parameter and transformation matrices based on the kinematic modeling were established to calculate the workspace; the volume of the alpha shape was calculated to quantify the workspace.

As a result, the workspace with the proposed system expanded approximately 8.40 times in the inward mode. In addition, the joint torque of the human hand was reduced by 21.14 %. The delay occured when the MAH system operated in the inward mode, which was also measured experimentally. The results of the experiment with 2D tracking analysis indicated that the average delay difference between the grasping intention and actuator operation was 0.048 s.

Unlike previous finger exoskeleton systems, the fingers of the MAH system do not contact with human fingers because they are not directly mounted on the human fingers [13]–[21]. Therefore, the wearer can move their fingers freely and has little risk of injury caused by the robot. Furthermore, the MAH system has three robotic fingers, which reduce the load on the human fingers more than the additive finger system with one or two robotic fingers [22], [24]–[26]. In addition, using the second palm mounted on the back of the human hand, the MAH system creates a new space for grasping objects and maximizing the workspace of the hand. The previous exoskeleton systems mainly use the EMG

signal to control the system with the feedback from human body [25], [26]. The MAH system uses the piezoelectric sensor, which is smoothly attached to the human wrist and sends the sensing signal from the wrist skin. Therefore, the operating process is simple and the delay time is only 0.048 s on average.

One thing that needs to be improved was found when wearing and operating the MAH system. The finger 2 of the MAH system which is located between the thumb and wrist was verified to collide with the thumb in specific operating situation. This problem was not recognized when conducting simulation because the kinematic models do not reflect the volume of the muscle and skin of the thumb, and the width of the robotic finger as shown in Fig. 10. If the design of the proposed system is modified so that the finger 2 is located closer to the wrist, its workspace will not overlap with that of the human thumb, and the grasping performance will also be improved.

ACKNOWLEDGMENT

The authors would like to thank Chaewon Oh for her help with drawing schematic.

REFERENCES

[1] J. Napier, J. R. Napier, and R. H. Tuttle, *Hands*, vol. 9. Princeton, NJ, USA: Princeton Univ. Press, 1993.

[2] R. Diogo, B. G. Richmond, and B. Wood, "Evolution and homologies of primate and modern human hand and forearm muscles, with notes on thumb movements and tool use," *J. Human Evol.*, vol. 63, no. 1, pp. 64–78, Jul. 2012.

[3] S. Almécija, J. B. Smaers, and W. L. Jungers, "The evolution of human and ape hand proportions," *Nature Commun.*, vol. 6, no. 1, pp. 1–11, Nov. 2015.

[4] O. J. Lewis, "Joint remodelling and the evolution of the human hand," *J. Anatomy*, vol. 123, no. 1, p. 157, 1977.

[5] S. L. Kilbreath and R. C. Heard, "Frequency of hand use in healthy older persons," *Austral. J. Physiotherapy*, vol. 51, no. 2, pp. 119–122, 2005.

[6] A. Saudabayev, Z. Rysbek, R. Khassenova, and H. A. Varol, "Human grasping database for activities of daily living with depth, color and kinematic data streams," *Sci. Data*, vol. 5, no. 1, Dec. 2018, Art. no. 180101.

[7] P. W. Ferguson, Y. Shen, and J. Rosen, "Hand exoskeleton systems—Overview," in *Wearable Robotics*. Amsterdam, The Netherlands: Elsevier, 2020, pp. 149–175.

[8] B. Noronha and D. Accoto, "Exoskeletal devices for hand assistance and rehabilitation: A comprehensive analysis of state-of-the-art technologies," *IEEE Trans. Med. Robot. Bionics*, vol. 3, no. 2, pp. 525–538, May 2021.

[9] K. Kiguchi and Y. Hayashi, "An EMG-based control for an upper-limb power-assist exoskeleton robot," *IEEE Trans. Syst., Man, Cybern. B, Cybern.*, vol. 42, no. 4, pp. 1064–1071, Aug. 2012.

[10] R. A. R. C. Gopura and K. Kiguchi, "Mechanical designs of active upper-limb exoskeleton robots: State-of-the-art and design difficulties," in *Proc. IEEE Int. Conf. Rehabil. Robot.*, Jun. 2009, pp. 178–187.

[11] Z. Li, B. Wang, F. Sun, C. Yang, Q. Xie, and W. Zhang, "SEMG-based joint force control for an upper-limb power-assist exoskeleton robot," *IEEE J. Biomed. Health Informat.*, vol. 18, no. 3, pp. 1043–1050, May 2014.

[12] T. Noda, T. Teramae, B. Ugurlu, and J. Morimoto, "Development of an upper limb exoskeleton powered via pneumatic electric hybrid actuators with bowden cable," in *Proc. IEEE/RSJ Int. Conf. Intell. Robots Syst.*, Sep. 2014, pp. 3573–3578.

[13] P. Agarwal, J. Fox, M. K. O'Malley, A. D. Deshpande, and Y. Yun, "An index finger exoskeleton with series elastic actuation for rehabilitation: Design, control and performance characterization," *Int. J. Robot. Res.*, vol. 34, no. 14, pp. 1747–1772, Oct. 2015.

[14] P. S. Lum, S. B. Godfrey, E. B. Brokaw, R. J. Holley, and D. Nichols, "Robotic approaches for rehabilitation of hand function after stroke," *Amer. J. Phys. Med. Rehabil.*, vol. 91, no. 11, pp. S242–S254, 2012.

[15] P. Heo, G. M. Gu, S. Lee, K. Rhee, and J. Kim, "Current hand exoskeleton technologies for rehabilitation and assistive engineering," *Int. J. Precis. Eng. Manuf.*, vol. 13, no. 5, pp. 807–824, May 2012.

[16] J. Iqbal, N. G. Tsagarakis, and D. G. Caldwell, "A multi-DOF robotic exoskeleton interface for hand motion assistance," in *Proc. Annu. Int. Conf. IEEE Eng. Med. Biol. Soc.*, Aug. 2011, pp. 1575–1578.

[17] S. Ueki, H. Kawasaki, S. Ito, Y. Nishimoto, M. Abe, T. Aoki, Y. Ishigure, T. Ojika, and T. Mouri, "Development of a hand-assist robot with multi-degrees-of-freedom for rehabilitation therapy," *IEEE/ASME Trans. Mechatronics*, vol. 17, no. 1, pp. 136–146, Feb. 2012.

[18] A. Chiri, M. Cempini, S. M. M. De Rossi, T. Lenzi, F. Giovacchini, N. Vitiello, and M. C. Carrozza, "On the design of ergonomic wearable robotic devices for motion assistance and rehabilitation," in *Proc. Annu. Int. Conf. IEEE Eng. Med. Biol. Soc.*, Aug. 2012, pp. 6124–6127.

[19] H. K. Yap, J. Hoon Lim, F. Nasrallah, J. C. H. Goh, and R. C. H. Yeow, "A soft exoskeleton for hand assistive and rehabilitation application using pneumatic actuators with variable stiffness," in *Proc. IEEE Int. Conf. Robot. Autom. (ICRA)*, May 2015, pp. 4967–4972.

[20] J. Yi, Z. Shen, C. Song, and Z. Wang, "A soft robotic glove for hand motion assistance," in *Proc. IEEE Int. Conf. Real-Time Comput. Robot. (RCAR)*, Jun. 2016, pp. 111–116.

[21] P. Polygerinos, Z. Wang, K. C. Galloway, R. J. Wood, and C. J. Walsh, "Soft robotic glove for combined assistance and at-home rehabilitation," *Robot. Auto. Syst.*, vol. 73, pp. 135–143, Nov. 2015.

[22] D. Prattichizzo, M. Malvezzi, I. Hussain, and G. Salvietti, "The sixth-finger: A modular extra-finger to enhance human hand capabilities," in *Proc. 23rd IEEE Int. Symp. Robot Hum. Interact. Commun.*, Aug. 2014, pp. 993–998.

[23] G. Gu, N. Zhang, H. Xu, S. Lin, Y. Yu, G. Chai, L. Ge, H. Yang, Q. Shao, X. Sheng, X. Zhu, and X. Zhao, "A soft neuroprosthetic hand providing simultaneous myoelectric control and tactile feedback," *Nature Biomed. Eng.*, pp. 1–10, Aug. 2021.

[24] T. Lisini Baldi, N. D'Aurizio, C. Gaudeni, S. Gurgone, D. Borzelli, A. D'Avella, and D. Prattichizzo, "Exploiting implicit kinematic kernel for controlling a wearable robotic extra-finger," 2020, *arXiv:2012.03600*.

[25] R. Ismail, M. Ariyanto, K. A. Pambudi, J. W. Syafei, and G. P. Ananto, "Extra robotic thumb and exoskeleton robotic fingers for patient with hand function disability," in *Proc. 4th Int. Conf. Electr. Eng., Comput. Sci. Informat. (EECSI)*, Sep. 2017, pp. 1–6.

[26] I. Hussain, G. Spagnoletti, and G. Salvietti, "Toward wearable supernumerary robotic fingers to compensate missing grasping abilities in hemiparetic upper limb," *Int. J. Robot. Res.*, vol. 36, nos. 13–14, pp. 1414–1436, Jul. 2017.

[27] K. M. Lynch and F. C. Park, *Modern Robotics*. Cambridge, U.K.: Cambridge Univ. Press, 2017.

[28] L. Radavelli, R. Simoni, P. E. De, and D. Martins, "A comparative study of the kinematics of robots manipulators by Denavit–Hartenberg and dual quaternion," *Mecánica Comput., Multi-Body Syst.*, vol. 31, no. 15, pp. 2833–2848, 2012.

[29] S. Cobos, M. Ferre, M. A. Sanchez Uran, J. Ortego, and C. Pena, "Efficient human hand kinematics for manipulation tasks," in *Proc. IEEE/RSJ Int. Conf. Intell. Robots Syst.*, Sep. 2008, pp. 2246–2251.

[30] S. B. Backus and A. M. Dollar, "An adaptive three-fingered prismatic gripper with passive rotational joints," *IEEE Robot. Autom. Lett.*, vol. 1, no. 2, pp. 668–675, Jul. 2016.

[31] A. Konno, M. Tada, K. Nagashima, M. Inaba, and H. Inoue, "Development of a 3-fingered hand and grasping unknown objects by groping," in *Proc. IEEE Int. Symp. Assem. Task Planning*, Aug. 1997, pp. 72–77.

[32] Y. Xin, H. Sun, H. Tian, C. Guo, X. Li, S. Wang, and C. Wang, "The use of polyvinylidene fluoride (PVDF) films as sensors for vibration measurement: A brief review," *Ferroelectrics*, vol. 502, no. 1, pp. 28–42, Sep. 2016.

[33] A. Proto, K. Vlach, S. Conforto, V. Kasik, D. Bibbo, D. Vala, I. Bernabucci, M. Penhaker, and M. Schmid, "Using PVDF films as flexible piezoelectric generators for biomechanical energy harvesting," *Lékař Technika-Clinician Technol.*, vol. 47, no. 1, pp. 5–10, 2017.

[34] Z. Shen, F. Chen, X. Zhu, K.-T. Yong, and G. Gu, "Stimuli-responsive functional materials for soft robotics," *J. Mater. Chem. B*, vol. 8, no. 39, pp. 8972–8991, 2020.

[35] B. Dutta, E. Kar, N. Bose, and S. Mukherjee, "NiO@SiO_2/PVDF: A flexible polymer nanocomposite for a high performance human body motion-based energy harvester and tactile e-skin mechanosensor," *ACS Sustain. Chem. Eng.*, vol. 6, no. 8, pp. 10505–10516, Aug. 2018.

[36] W. Dong, L. Xiao, W. Hu, C. Zhu, Y. Huang, and Z. Yin, "Wearable human–machine interface based on PVDF piezoelectric sensor," *Trans. Inst. Meas. Control*, vol. 39, no. 4, pp. 398–403, 2017.
[37] D. Dragulescu, V. Perdereau, M. Drouin, L. Ungureanu, and K. Menyhardt, "3D active workspace of human hand anatomical model," *Biomed. Eng. OnLine*, vol. 6, no. 1, p. 15, Dec. 2007.
[38] H. Kjnoshita, S. Kawai, and K. Ikuta, "Contributions and co-ordination of individual fingers in multiple finger prehension," *Ergonomics*, vol. 38, no. 6, pp. 1212–1230, Jun. 1995.
[39] J. D. Gardiner, J. Behnsen, and C. A. Brassey, "Alpha shapes: Determining 3D shape complexity across morphologically diverse structures," *BMC Evol. Biol.*, vol. 18, no. 1, p. 184, Dec. 2018.
[40] X. Jiang, S. Lou, and P. J. Scott, "Morphological method for surface metrology and dimensional metrology based on the alpha shape," *Meas. Sci. Technol.*, vol. 23, no. 1, Jan. 2012, Art. no. 015003.
[41] X. Xu and K. Harada, "Automatic surface reconstruction with alpha-shape method," *Vis. Comput.*, vol. 19, nos. 7–8, pp. 431–443, Dec. 2003.
[42] L. Li, S. Rui, Q. Nie, X. Gong, and F. Li, "Conformal alpha shape-based multi-scale curvature estimation from point clouds," *J. Comput.*, vol. 7, no. 6, pp. 1460–1466, 2012.

KANGHYEON LEE received the B.S. degree in mechanical and aerospace engineering from Seoul National University, Seoul, South Korea, where he is currently pursuing the M.S. degree in mechanical engineering. He was a Student Researcher with the Center for Intelligent and Interactive Robotics, Korea Institute of Science and Technology, Seoul. He is currently a Researcher with the School of Electrical Engineering, Korea University, Seoul. His research interests include biomimetic robotics and modeling of mechatronic systems.

PYEONG-GOOK JUNG received the B.Eng., M.S., and Ph.D. degrees in mechanical engineering from Sogang University, Seoul, South Korea, in 2013, 2015, and 2019, respectively. His current research interests include wearable robotics, rehabilitation robotics, human intention recognition devices, and soft mechatronics.

YEONSEO LEE received the B.S. degree from the Division of Robotics, Kwangwoon University, Seoul, South Korea. She is currently pursuing the M.S. degree with the KAIST Robotics Program. She was a Research Trainee with the Center for Intelligent and Interactive Robotics, Korea Institute of Science and Technology (KIST), Seoul. Her current research interests include soft mechatronics, wearable robotics, and teleoperation systems.

YOUNGSU CHA (Senior Member, IEEE) received the B.S. degree in electrical engineering from Korea University, Seoul, South Korea, in 2004, the M.S. degree in electrical engineering from the Korea Advanced Institute of Science and Technology (KAIST), Daejeon, South Korea, in 2007, and the Ph.D. degree in mechanical engineering from New York University, New York, NY, USA, in 2015. He was a Principal Research Scientist with the Center for Intelligent and Interactive Robotics, Korea Institute of Science and Technology (KIST), Seoul. He is currently an Assistant Professor with the School of Electrical Engineering, Korea University. His current research interests include smart materials and structures, multiphysics modeling, flexible sensors and actuators, energy harvesting, and robotics.